Time-dependent Pinning of Nanoblisters Confined by Two-dimensional Sheets. Part 2: Contact Line Pinning

Chengfu Ma,[1,2,*] Yuhang Chen,[2,*] and Jiaru Chu[1,2]

[1] *CAS Key Laboratory of Mechanical Behavior and Design of Materials, Department of Precision Machinery and Precision Instrumentation, University of Science and Technology of China, Hefei 230026, China*

[2] *Key Laboratory of Precision Scientific Instrumentation of Anhui Higher Education Institutes, Department of Precision Machinery and Precision Instrumentation, University of Science and Technology of China, Hefei 230026, China*

(Dated: December 08, 2022)

ABSTRACT: Pinning of droplets on solids is an omnipresent wetting phenomenon that attracts intense research interests. Unlike in classical wetting, pinning effects in a novel wetting problem where droplets are confined onto the substrates by elastic films have hardly been investigated. Here, following our study in an accompanying paper (Part 1) on the static mechanics of nanoscale blisters confined between a two-dimensional elastic sheet and its substrate, we investigate in this Part the pinning behaviors of such blisters by using atomic force microscopy. The blisters' lateral retention forces are shown to scale almost linearly with their contact lines and to increase until saturations with increasing their resting times. Our analysis reveals a mechanism of micro-deformation of the substrate at the contact line. Creep of the micro-deformation is found to cause the time-dependent pinning, which is evidenced by residual fine ridge structures left by blisters after their spreads after long resting times.

Keywords: elastic-wetting; blister; pinning; 2D materials; atomic force microscopy

INTRODUCTION

Wetting of solids by liquids is an omnipresent phenomenon in nature and in daily life, and is also of great importance in many industrial applications such as self-cleaning surfaces, oil/water separation, and directional liquid transport. It thus has been a longstanding subject with rich results, yet still receives intense investigations [1]. In contrast to the classical wetting on solid surfaces, a novel wetting problem where droplets are confined onto substrates by elastic thin films draws attention only recently. Such wetting phenomena can be observed over a wide range of length scales, for example as domes formed by epithelia cells [2], and as nanoscale blisters trapped in the interfaces between two-dimensional (2D) materials and their substrates [3–9]. In this kind of wetting, the elasticity of the capping film plays a role in governing the wetting behavior together with the surface tensions. For example, it has been shown that the morphology and the contact angle of a droplet capped by an elastic film can be tuned by adjusting the tension applied in the capping film [10]. It is therefore termed as elastic-wetting elsewhere [11].

To understand the difference between the elastic-wetting problem and the classical wetting, Rao *et al* has theoretically studied the configurations of membrane-confined droplets in equilibrium for different boundary conditions [11]. However, other behaviors of elastic-wetting have hardly been explored. Among them, one significant concern is how the confined droplet pins in the interfaces and how it starts to slide (depinning). In fact, this is also a major question in recent classical wetting researches that draws interests from the community [12–19]. Understanding the pinning behaviors of confined droplets is not only academically important, but also is key for practical issues. For example, it is no doubt of beneficial for developing methods of cleaning interfacial blisters trapped in van der Waals (vdW) heterostructures, which are detrimental for their performances [8, 20–22].

Here, in this work, we investigate the pinning behaviors of nanoscale blisters confined between a 2D elastic sheet and its substrate by using atomic force microscopy (AFM). Our study on the static mechanics of such blisters can be found in an accompanying paper (Part 1) [23], which is essential for the analyses in this Part. Sealing of droplets by the 2D sheet makes manipulating them and measuring their pinning forces by an AFM probe possible. This brings the study of pinning effect of wetting into the micro- and nanometer scales. Our results reveal a time-dependent pinning effect of the confined blisters. The blisters' lateral retentions forces are found to increase with increasing their resting times until saturations. Our analysis suggests that dissipations by fine deformations of the substrate, induced by vertical tensions at the contact lines, play important roles in the blisters' pinning. The creep of the deformation is suggested to result in the time-dependence of the blisters' pinning, as well as the observed residual ridge structures left by blisters at their original contact lines after their spreads after long resting times.

* Corresponding authors: chfuma@ustc.edu.cn (C. M.); chenyh@ustc.edu.cn (Y. C.)

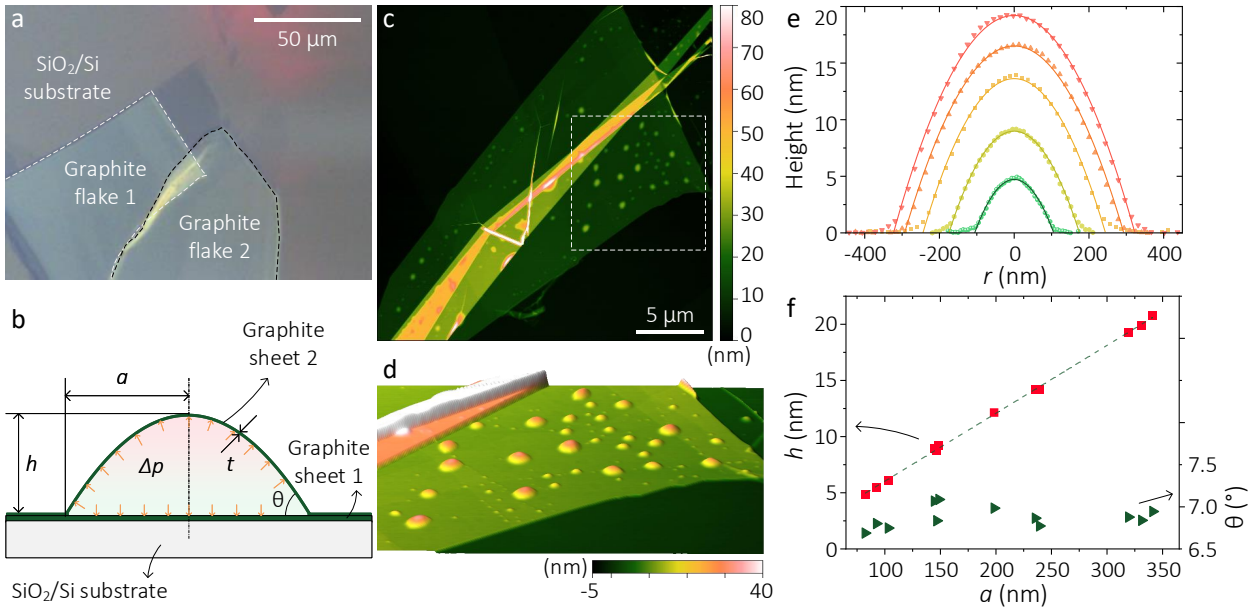

FIG. 1. Shape characteristics of the confined blisters. (a) The optical image of two overlaying graphite flakes on the SiO_2/Si substrate; (b) A schematic model of the confined blister; (c) AFM topography of the overlay area of the two flakes; (d) 3D display of the encased area in (c); (e) AFM height profiles across the centers of typical blisters (data points), fitted by the assumed deflection for a pressurized membrane; (f) The measured central heights h (square points), and the contact angles θ (triangle points) as a function of the radii a for various blisters.

EXPERIMENTAL SECTION

Sample Preparation. Nanoscale blisters that are spontaneously formed between two thin graphite sheets lying on a SiO_2/Si substrate are used for study. The sample was fabricated by mechanically exfoliating graphite and graphene flakes from a natural graphite sample and then transferring them onto the SiO_2/Si substrate by using the Scotch Tape method [24]. The SiO_2/Si substrate has an oxide layer thickness of 90 nm. The sample was prepared and kept in normal room temperature and humidity conditions. More information on the sample can be found in Part 1 [23].

Measurement Methods. All the AFM measurements and manipulations were carried out on a commercial AFM (Dimension Icon, Bruker, CA). Three silicon cantilevers (ContAl-G, Budget-Sensors, Bulgaria) were used in the measurements. Their spring constants were calibrated to be respectively 0.24, 0.33, 0.30 N/m by using the thermal noise method [25]. The curvature radii of the tips were measured to be approx. 17.8, 23.4, and 18.5 nm after all the experiments by using a scanning helium ion microscope (ORION NanoFab, ZEISS), see Fig. S1 in the supporting information (SI). The blisters' topographies were acquired locally before their manipulations with tip loads as small as possible. Their manipulations were carried out by contact mode scanning with a scan rate of 5 μm/s in scan sizes ranging over 200∼900 nm^2 depending on their sizes. The adhesion forces measured on the graphite flakes before each manipulation were included in the measured tip loads, which range over 3∼4 nN.

RESULTS AND DISCUSSION

Shape Characteristics of the Confined Blisters. As shown in the optical and AFM topography images in Figs. 1(a) and 1(c), blisters that are spontaneously formed between two overlaying graphite flakes on a SiO_2/Si are used for study in this work. A schematic illustration of such a blister can be seen in Fig. 1(b). Such blisters are indeed frequently observed between 2D materials and their substrates [3–9, 20–22]. Studies have suggested that liquid water is the most likely substance inside the blisters [3–8, 22]. Our observation of residual wetting ridge structures in this work provides further evidence that the confined substance in our sample is liquid. The blisters are determined to be confined between the two graphite flakes since the graphite-SiO_2 interface is found holding no such features. In fact, for our sample, we observe confined blisters only at graphite (or multilayer graphene)-graphite interfaces (see Part 1 [23]). The two flakes are determined to have almost the same thickness of approx. 8.6 nm by measuring their step heights by AFM at their edges.

As can be seen from Fig. 1(d), the blisters span over a large size scale. However, for simplicity, our study is carried out on a number of blisters having central heights that are at least three times larger than an effective length scale $h_e = \sqrt{12(1-\nu^2)D/K} = \sqrt{E/E_{in}t} \sim 1.6$ nm. Here, $D = Et^3/12(1-\nu^2)$ is the flexural rigidity of the capping sheet, $K = E_{in}t$ is defined as its in-plane elastic stiffness, in which E=36.5 GPa and ν=0.16 are respectively the Young's modulus and Poisson's ratio, E_{in}=1.06 TPa is its in-plane Young's modulus of

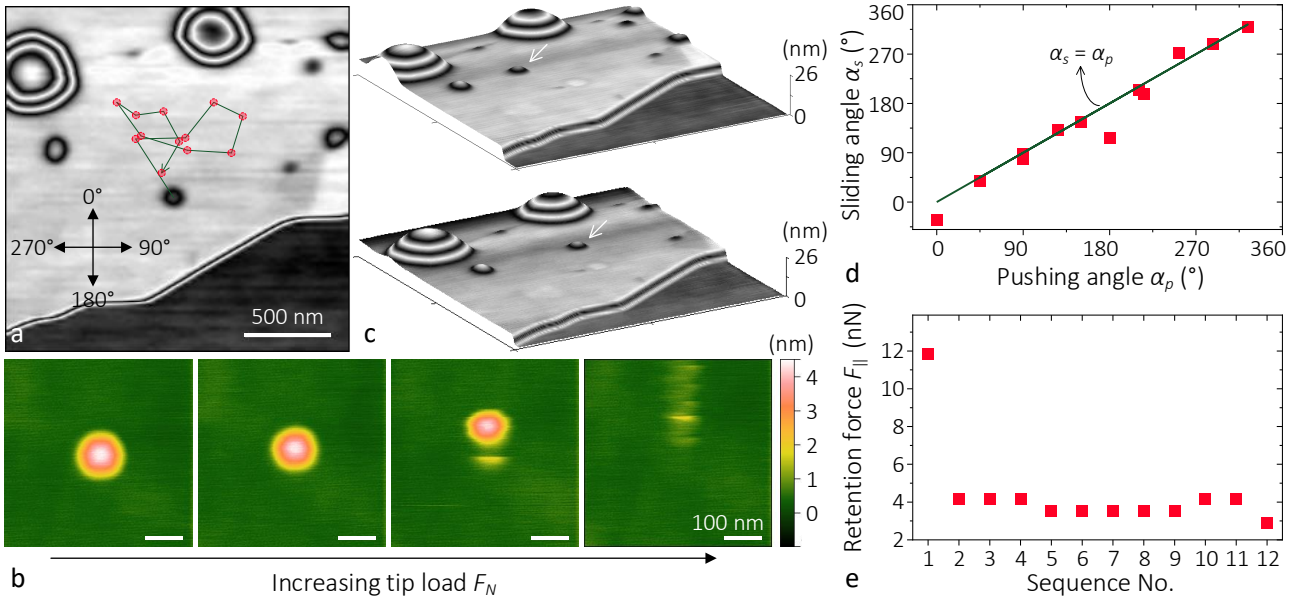

FIG. 2. **Manipulating the blister and measuring its retention force.** (a) AFM topography of an area containing several blisters, in which the slow scan coordinate and the center blister's trajectory in subsequent motions are illustrated; (b) Typical AFM topographies of the center blister in (a) under increased scanning tip loads; (c) 3D displays of the AFM topographies of the same area in (a) showing the center blister's different locations after motions; (d) The actual sliding angles α_s measured for various pushing angles α_p (data points), and a solid line representing α_s=α_p; (e) The measured lateral retention forces $F_{\|}$ for the 12 motions of the blister.

the lamellar graphite, as adopted from [26], and t=8.6 nm is its thickness. Blisters that meet the above circumstance are expected to be in the membrane regime, and their central height profiles are expected to follow the assumed deflection of a pressurized membrane, $w(r) = h(1 - r^2/a^2)$ (see Refs. [27, 28] and Part 1 [23]). Here, h and a are respectively the center height and the capping radius, as illustrated in Fig. 1(b). Indeed, for the blisters studied here, their central height profiles are well described by this assumed deflection form, which can be seen from the curve fittings in Fig. 1(e) of central height profiles representing typical blisters from the largest to the smallest.

Then, by applying curve fittings with the assumed deflection equation above to the central height profiles of the blisters, their radii a and center heights h are measured. It should be mentioned that the studied blisters are chosen to be relatively far from steps or other interfaces defects. Most of the studied blisters have near round shapes, with ∼70% of them having an original mean major-to-minor-axes aspect ratio of 1.09±0.04. However, measurements on a few elliptical blisters with major-to-minor-axes aspect ratios of 1.18∼1.35 are also included considering that shape changes may be inevitable after manipulations in latter experiments. Therefore, the shape characteristics of the blisters, a and h, reported in this work are obtained from the angularly averaged radial profiles of the blisters. The Gwyddion software was used to analyze the major-to-minor-axes aspect ratio of the blisters, as well as to extract their angularly averaged radial profiles. In addition, it should be noted that corrections were done for a to deduce the tip dilations as well as to define it from the middle plane of the sheet by subtracting half the sheet thickness $t/2$ (see section 2.1 in the SI). The resulting central heights h of the blisters are shown in Fig. 1(f) as a function of their radii a, from which a linear relation between them, i.e. a constant aspect ratio $h/a \sim 0.060\pm0.001$, is observed. This indicates that the blisters have almost the same contact angle $\theta \sim 6.88\pm0.12°$, as shown in Fig. 1(f), since we have $\tan\theta = 2h/a$ from the deflection equation. Such a scaling law is indeed also observed for blisters confined in various interfaces [3, 6, 7, 9], and is well explained by our theorical analysis in Part 1 [23].

Retention Force Measurement. Next, we investigate the pinning effects of the blisters by manipulating them horizontally with contact mode AFM. The retention forces, that are the threshold forces required to initiate the blisters' motions are measured. For this purpose, a blister of interest is first located in an area that contains it by imaging with a tip load as small as possible, for example for the one at the center of Fig. 2(a). Then it is manipulated locally to avoid interferences with other blisters and blemishes such as steps. As demonstrated in Fig. 2(b), in order to measure its retention force, repeated scans are carried out with increasing the tip loads F_N each time by a step of approx. 6.1 nN. The blister is found to stay steady at small loads, and starts to slide at a threshold tip load. An example of such a motion

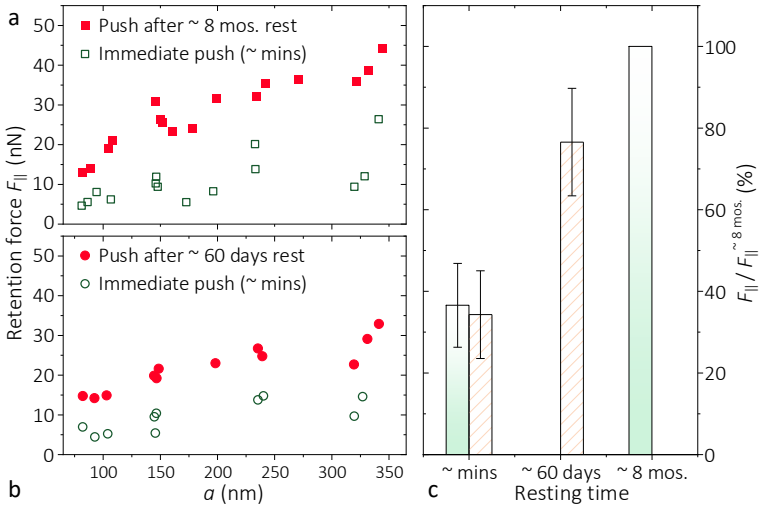

FIG. 3. Retention forces measured for various resting times. The lateral retention forces $F_{\parallel}$ of a number of blisters as functions of their radii a measured for their first and subsequent immediate motions (∼minutes) after a resting time of (a) ∼8 months and (b) ∼60 days; (c) The mean values of the blisters' retention forces normalized by their corresponding ones for ∼8 months, with the error bars standing for standard deviations among blisters. The columns with slashes stand for the case in (b) and the others for (a).

is displayed in Fig. 2(c). The lateral retention force $F_{\parallel}$ is then calculated from the threshold tip load from a decomposition of forces, see section 2.1 in the SI for details.

To examine whether there exists an anisotropy for the blisters' motion, we consecutively push the same blister towards all directions and record its sliding angles and retention forces. In Fig. 2(a), we show the blister's resting locations after 12 motions, where the corresponding AFM images are given in the SI (Fig. S2). The sliding angles are calculated from the resting locations in the same coordinate illustrated in Fig. 2(a). As can be seen from Fig. 2(d), the actual sliding angles coincide well with the pushing angles which are defined by the AFM slow scan directions. In addition, from the measured retention forces shown in Fig. 2(e), we see that except for the first motion, the retention forces change little for manipulations towards various directions. This implies that the motion of the blister in the graphite-graphite interface is isotropic.

Time-dependence of the Retention Force. It's very interesting to see the significantly larger retention force of the blister for its first motion than the ones for subsequent immediate motions (Fig. 2(e)). This implies a possible pinning effect that depends on the blister's resting history. To further verify this observation, we measured the retention forces of a number of blisters for their first and followed immediate motions. It should be mentioned that a few blisters have coalesced or been squeezed out of the interface (see Fig. S3 in the SI), therefore they were not studied in further experiments. Before their first motions, the blisters have stayed undisturbed for almost 8 months since the sample fabrication. However, they rested only a few minutes at their new locations before the subsequent motions. The results are shown in Fig. 3(a). For all the blisters, the retention forces are found to be significantly decreased for the following motions compared to their first motions. This surprising phenomenon is again observed in Fig. 3(b) for repeating the experiments after leaving the blisters undisturbed for about 60 days. It can be found that the retention forces have recovered notably after the 60 days' resting. Then once they are moved again, the retention forces drop in a manner as in Fig. 3(a).

Here, we compare the retention forces of the blisters as a function of the resting time to reveal its effect more clearly. To do so, the retention forces of the blisters $F_{\parallel}$ are normalized by their respective $F_{\parallel}^{\sim 8mos.}$ for resting times of ∼ 8 months. From the statistical results shown in Fig. 3(c), one can see that for both cases having resting times of only a few minutes, the blisters experienced equivalent retention forces that are as small as ∼ 35% of their $F_{\parallel}^{\sim 8mos.}$. Then by increasing the resting time to ∼ 60 days, the retention forces increased to ∼ 77% of their $F_{\parallel}^{\sim 8mos.}$. The results unambiguously illustrate that pinning of those blisters is indeed dependent on their resting time. Additionally, one can see from both Figs. 3(a) and 3(b) generally linear relations between the retention forces and the blisters' radii for all cases, which indicate a length-dependent rather than an area-dependent pinning behavior.

Residual Fine Ridge Structures. What is the mechanism behind the time-dependent pinning of the blisters? In order to answer this question, we first rule out the possibilities of shape characteristics variations. The blisters' radii a and aspect ratios h/a are observed to vary little and therefore are hardly responsible for the time-dependence. Instead, we notice fine residual structures

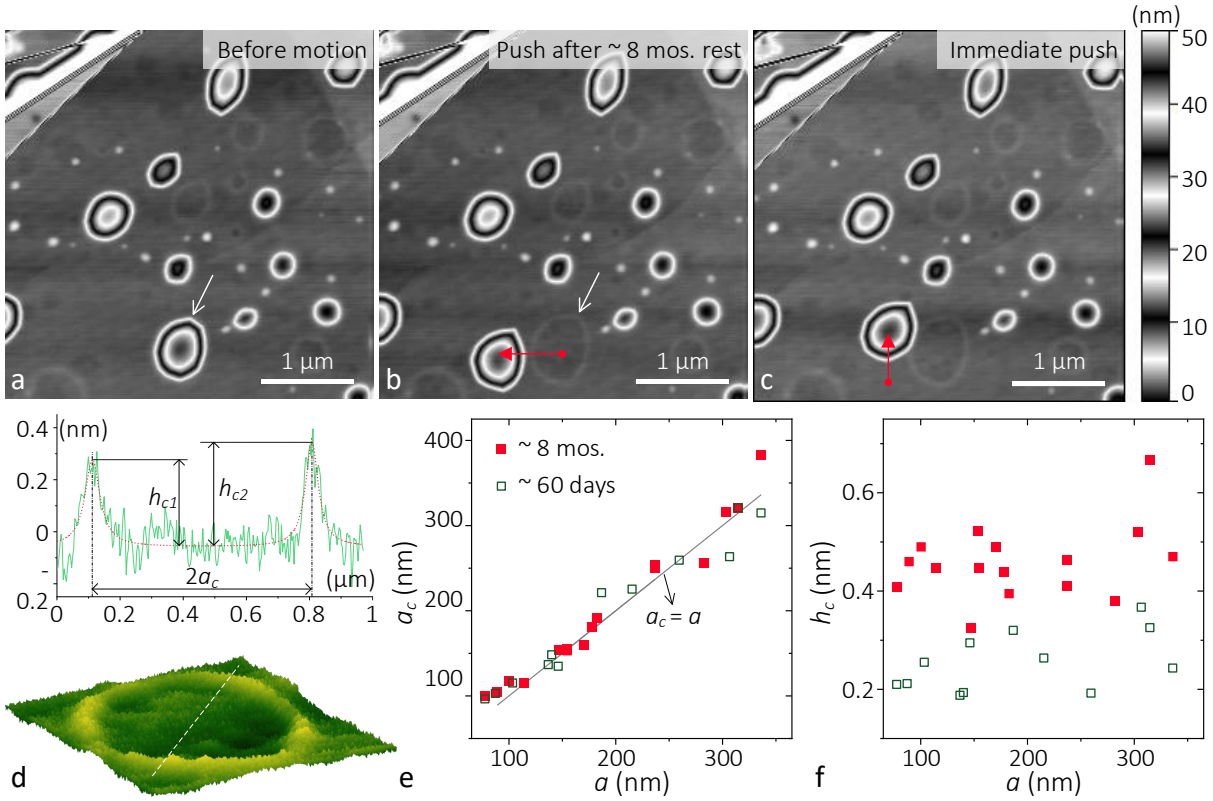

FIG. 4. Residual ridge structures left after blisters' motions. AFM topographies of an area (a) before and after the pointed blister being moved (b) after a resting time of ~ 8 mos. and (c) after a subsequent gap of a few minutes; (d) 3D display of the residual structure in (b) indicated by a white arrow, and its height profile across the center; (e) The residual structures' radii a_c and (f) heights h_c as functions of their corresponding blisters' radii a for the two resting time cases of ~ 8 mos. and ~ 60 days.

being left over after moving the blisters, whose emergences correlate with the resting times of the blisters. For example, when the blister pointed in Fig. 4(a) is moved as in Fig. 4(b) after a resting time of ~ 8 months, a ring ridge structure appears at the original spot. It is however not observed for a blister motion after a short resting time of a few minutes (Fig. 4(c)), but again emerges for a longer resting time of ~ 60 days (see Fig. S4 in the SI). More of such residual features left earlier by other blisters can also be seen in Figs. 4(a)-(c). Be aware of their correlations to the time-dependent pinning effect, here we characterize the residual features of corresponding blisters in Fig. 3. As illustrated in Fig. 4(d), the residual features present as fine ridge structures protruded from the substrate. From their central height profiles, we measure their radii a_c and heights $h_c = (h_{c1} + h_{c2})/2$ as defined in Fig. 4(d). From the resulted a_c as shown in Fig. 4(e), we conclude that the residual structures appear exactly at the blisters' circumferences before motions. This applies to both cases with resting times of ~ 60 days and ~ 8 mos.. In addition, we can see from Fig. 4(f) that the heights of the residual structures are of a few angstroms. The longer resting time ~ 8 mos. is found to induce residual structures with larger heights.

Wetting Ridge at the Contact Line and Its Influence on the Retention Force. The residual ridge structures emerged at the blisters' original circumferences after their motions are reminiscent of deformations of solid substrates induced by liquid droplets at the three phase contact lines [12, 13, 29–36]. Such deformations originate from the unbalanced vertical tensions in the classical Young–Dupré equation. The Young–Dupré equation describes the balance of interface tensions in the horizontal direction, however ignores the balance in the vertical. The latter then must be fulfilled by a tension provided by the substrate, which pulls the substrate to form a ridge-like structure at the contact line known as "wetting ridge" [29–31]. Such a wetting ridge is minuscule for a rigid substrate, but can be as high as tens of nanometers [31] or even a few micrometers [13] on soft surfaces. Its influences on macroscopic wetting behaviors are therefore of significant [12, 31, 32, 37].

Here, we employ this theory to our case to investigate the micro-deformation of the substrate and its effect on pinning. To do so, we first examine the tension balance at the contact line of a liquid droplet confined between an elastic sheet and a substrate. As illustrated in the left inset of Fig. 5(a), the radial tension τ in the elastic sheet

should be incorporated together with the interfacial tensions [10, 11]. Here, γ_{cb}, γ_{sb}, γ_{cs} represent respectively the interfacial tensions between the capping sheet ('c'), the blister substance ('b'), and the substrate ('s'). Similar to the classical Young–Dupré equation, a horizontal balance of the tensions defines the apparent contact angle θ as

$$\cos\theta = \frac{\gamma_{cs} - \gamma_{sb} + \tau}{\gamma_{cb} + \tau} = \frac{-\gamma_{gb} + \tau}{\gamma_{gb} + \tau}. \quad (1)$$

Here, in our case, the radial stretching tension τ in the capping sheet at the blister's edge is obtained as $\tau = K(h/a)^2/4$ from our analysis in Part 1 [23]. The capping sheet and the substrate are both graphite, we then assume the interfacial tension between them γ_{cs}=0, and γ_{cb}=γ_{sb}=γ_{gb}. In addition, since we have $\tan\theta = 2h/a$ from the blister's deflection profile, we derive $\gamma_{gb} \sim (h/a)^2\tau$ from Eq. (1) with a small-angle approximation for θ.

Next, we consider the vertical balance at the contact line. To fulfill the balance, a downward line tension from the substrate as below is must.

$$f_\perp = (\tau + \gamma_{gb})\sin\theta \approx \frac{K}{2}\left(\frac{h}{a}\right)^3\left[1 + \left(\frac{h}{a}\right)^2\right]. \quad (2)$$

Deformation of the substrate at the contact line is then expected. According to the calculation by Shanahan and De Gennes [38], a vertical line tension $f_\perp$ can result on an elastic substrate a wetting ridge with a height profile of

$$\xi(x) = \frac{2(1-\nu_s^2)f_\perp}{\pi E_s}\ln\left|\frac{d}{x}\right|, |x| > \epsilon. \quad (3)$$

Here, x is the distance from the contact line, $\xi(x)$ is defined for $|x| > \epsilon$ where ϵ is a cutoff length below which the deformation is no longer elastic, d is a distance where the deformation can be assumed to zero. E_s and ν_s are the Young's modulus and Poisson's ratio of the substrate.

For an almost constant aspect ratio of $h/a \sim 0.060$ in our experiments, we obtain a vertical traction of $f_\perp \sim$ 1.0 N/m at the contact line. If we treat the graphite substrate as an isotropic continuum material, then we get a wetting ridge height of $\sim$ 0.9 Å by assuming ϵ =1 nm and d =50 nm, as schematically illustrated in the right-hand inset of Fig. 5(a). However, this can only serve as a rough estimation since both parameters ϵ and d in Eq. (3) are hard to be defined precisely. In addition, graphite is actually a lamellar material which induces further complexity at this scale.

Let us now discuss how the microscopic deformation at the contact line affects the pinning of the latter. With the lateral spreading of a droplet, the wetting ridge accompanies by forming new ones at the fresh contact lines. Meanwhile, the substrate area that holds the original ridge restores its original configuration after the passage of the contact line (Fig. 5(b)). During this process, a fraction of the strain energy in the wetting ridge is expected to be dissipated in the lifting/releasing cycle. This then results in resistance for spreading of the droplet. For instance, for a viscoelastic substrate, the significant influence by the viscoelastic dissipation by the moving wetting ridge on the spreading dynamics of the droplet is well evidenced in classical wetting studies [13, 15, 31, 32, 39–41].

Here, for the graphite substrate, two mechanisms of energy loss maybe involved during the moving of its wetting ridge: viscoelastic process and interlayer friction, as suggested by a previous study [42] on the lateral displacement of adhesion-induced deformations on graphite. The exact fractions of these two kinds of dissipations are however hard to quantify. Therefore, here we regard them as one total dissipation which takes a χ fraction of the strain energy in the wetting ridge. The work done by the vertical tension (strain energy) during the moving of the wetting ridge has been calculated previously by Shanahan *et al* [39, 41]. Following their theory, we expect for our case a dissipation per unit time and per unit length as

$$\delta W_r = \chi\frac{2(1-\nu_s^2)(\tau+\gamma_{gb})^2 U}{\pi E_s \epsilon}, \quad (4)$$

Here, U is the advancing speed of the droplet. Other parameters are the same as in Eq. (3). Then, for an advancing distance of Δx, the dissipation by the entire wetting ridge having a perimeter of $2\pi a$ is derived as $\Delta W_r = \delta W_r \cdot 2\pi a \cdot \frac{\Delta x}{U}$. Considering a blister advancing in an equilibrium state, the wetting ridge dissipation ΔW_r is required to be balanced by an external work $F_{\parallel_r}\Delta x$. Here, $F_{\parallel_r}$is the retention force provided by the wetting ridge. From $F_{\parallel_r}\Delta x = \Delta W_r$, we obtain the pinning strength of the wetting ridge, that is the retention force per unit length, as

$$\frac{F_{\parallel_r}}{2\pi a} = \chi\frac{2(1-\nu_s^2)(\tau+\gamma_{gb})^2}{\pi E_s\epsilon} \sim \chi\frac{(1-\nu_s^2)K^2}{8\pi E_s\epsilon}\left(\frac{h}{a}\right)^4. \quad (5)$$

This then reveals a constant contact line pinning strength for the investigated blisters in our study considering that they have a constant aspect ratio h/a.

Besides the contact line pinning effect, resistances for moving a blister may also come from dissipations by the viscous flow of the liquid, blemishes at the solid-liquid interfaces, the debonding-bonding of the capping sheet from the substrate at the advancing front and rear, as well in the capping sheet. A complete investigation of these contributions is very challenging. However, considering the generally linear dependence of the measured retention forces $F_\parallel$ on the blisters' radii a, and especially the correlation between the residual wetting ridges and the significantly increased retention forces (Fig. 3), we suggest that the wetting ridges play major roles in the retention forces of the blisters. Therefore, here in this work we focus on the contact line pinning effect induced by the wetting ridge.

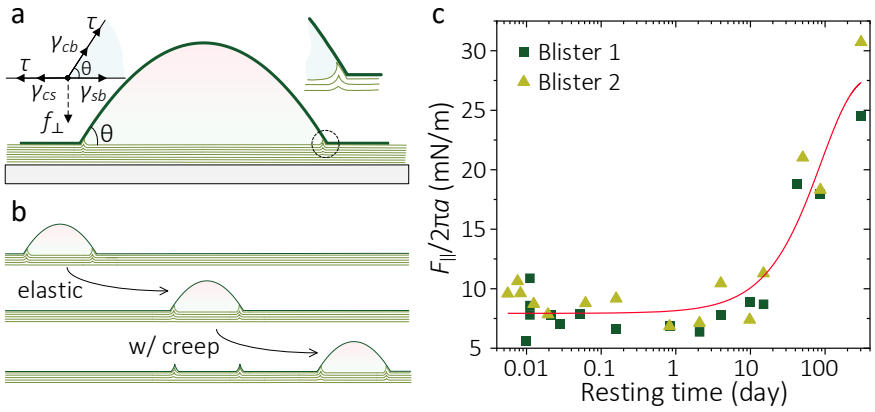

FIG. 5. Time-dependent substrate deformation at the contact line and its influence on blister pinning. (a) The schematic model of a blister confined by an elastic sheet onto a substrate. The left inset shows the tension balance at the contact line, and the right inset depicts a wetting ridge formed on the substrate at the contact line by the vertical tension; (b) Illustrations for advancing the blister with respectively a pure elastic wetting ridge and a wetting ridge containing creep. (c) The measured (data points) pinning strengths of two blisters as functions of their resting times and a fitting curve to all the data by the SLS model. The blisters have radii of 148.6 (blister 1) and 146.4 nm (blister 2).

Creep of Wetting Ridge and Time-dependent Pinning. The observation of time-dependent residual ridge structures in Fig. 4 implies creep deformations in the wetting ridges. As discussed before, under the vertical traction at the contact line, the substrate deforms and produces a wetting ridge. As illustrated in Fig. 5(b), for relatively short resting time, the wetting ridge deformation is mainly elastic and no residual structure is left after the passage of the blister. However, by increasing the persisting time of the traction, the material in the ridge creeps gradually, resulting in irreversible plastic deformation that remains after removing the traction. Since creep is a time-dependent deformation, it explains our observations in Fig. 4 that residual structures are only seen for the cases of long resting times $\sim$ 60 days and $\sim$ 8 mos.. Moreover, the larger heights of the residual ridges of $\sim$ 8 mos. than those of $\sim$ 60 days are also expected by this mechanism.

Here, let us discuss how the creep of a wetting ridge influences its pinning effect. With creep develops in the wetting ridge, more energy is dissipated in the cycle of lifting/releasing it, implying a larger work to advance it. The larger retention forces measured for blisters having longer resting times (Fig. 3) support this mechanism. Here, considering a standard linear solid (SLS) model, we expect a time-dependent creep compliance in the form of $J(t) = 1/E_s(t) = J_0 + J_1(1 - e^{-t/T})$ to replace the factor $1/E_s$ in Eq. (5). Here, J_0 and $J_\infty = J_0 + J_1$ are respectively the compliances at t=0 and t=∞, and T is the retardation time. This then results in a same time-dependent form for the wetting ridge induced retention force $F_{\|r}$, as well as for the total retention force $F_{\|}$ assuming that the additional retention force due to other dissipations is time-independent.

To verify this mechanism, we measured the retention forces $F_{\|}$ of two blisters for various resting times. The blisters have very close radii a of 148.6 (blister 1) and 146.4 nm (blister 2). Their resulting pinning strengths $F_{\|}/2\pi a$ are shown in Fig. 5(c) as functions of their resting times. It can be seen that the two blisters experience quite close pinning strengths, which is expectable from their almost same sizes. Additionally, their pinning strengths are found to increase in a very similar tendency with increasing their resting times. For resting times smaller than a few days, the changes of the retention forces are negligible, indicating minimal creep deformations in the wetting ridges. However, the retention forces are seen to increase significantly from a resting time of $\sim$ 10 days and to plateau after a resting time of a few hundred days. By fitting the data of both blisters by the SLS model as shown in Fig. 5(c), we can see that the time-dependent pinning effect of the blisters indeed agrees quite well the creep mechanism. The fitting yields pinning strengths of $\sim$ 7.9 mN/m at t=0, $\sim$ 28.0 mN/m at t=∞, as well as a retardation time of $T \sim 88\pm20$ days for the graphite substrate.

We aware that a previous work by N'guessan *et al* [43] has shown that the retention forces of water drops on graphene/graphite surfaces are invariant with the resting time, unlike experiments on some other surfaces where the retention forces increase with increasing the resting time, and reach plateaus typically after several minutes [15, 16]. However, their measurements are done for resting times of a few to $\sim$ 20 minutes, and our study suggests that such resting times maybe far too short to observe the time-dependent pinning effect on graphite.

CONCULSION

In summary, we have investigated the pinning of nanoscale blisters confined by a 2D elastic sheet by using AFM. Their retention forces were shown to scale almost linearly with the contact lines, and were further

demonstrated to increase with increasing their resting times until saturations. Fine residual ridge structures were observed at their original contact lines after moving the blisters for cases having long resting times. We concluded from the phenomena that the unbalanced vertical tensions at the contact lines of blisters pull the substrate to form ridge structures. The energy dissipations in such wetting ridges were found to play important roles in the blisters' retentions. The time-dependent pinning effects were suggested to result from creeps in the wetting ridges. The mechanism also explains the residues of permanent deformations left by blisters at their original contact lines after their spreads after long resting times.

ACKNOWLEDGMENTS

This work was supported by the National Natural Science Foundation of China (No. 52005476, 52075517) and the Hefei Municipal Natural Science Foundation (No. 2021014). We thank the USTC Center for Micro- and Nanoscale Research and Fabrication for technical support.

DATA AVAILABILITY

Data supporting the findings of this study are available from the corresponding author upon reasonable request.

CONFLICT OF INTEREST

The authors declare no competing financial interest.

SUPPORTING INFORMATION

Supplementary experimental data and theoretical analysis details supporting the findings of this work are available.

REFERENCES

[1] P. G. De Gennes, Wetting: statics and dynamics. *Reviews of modern physics*, **57**(3), 827 (1985).

[2] E. Latorre, S. Kale, L. Casares, M. Gómez-González, M. Uroz, L. Valon, R. V. Nair, E. Garreta, N. Montserrat, A. del Campo, L. Benoit, M. Arroyo, and T. Xavier, Active superelasticity in three-dimensional epithelia of controlled shape. *Nature*, **563**(7730), 203-208 (2018).

[3] P. Cao, K. Xu, J. O. Varghese, and J. R. Heath, The microscopic structure of adsorbed water on hydrophobic surfaces under ambient conditions. *Nano Letters*, **11**(12), 5581-5586 (2011).

[4] M. J. Lee, J. S. Choi, J. S. Kim, I. S. Byun, D. H. Lee, S. Ryu, C. Lee and B. H. Park, Characteristics and effects of diffused water between graphene and a SiO2 substrate. *Nano Research*, **5**(10), 710-717 (2012).

[5] C. H. Y. X. Lim, A. Sorkin, Q. Bao, A. Li, K. Zhang, M. Nesladek, and K. P. Loh, A hydrothermal anvil made of graphene nanobubbles on diamond. *Nature Communications*, **4**, 1556 (2013).

[6] M. Cheng, D. Wang, Z. Sun, J. Zhao, R. Yang, G. Wang, W. Yang, G. Xie, J. Zhang, P. Chen, C. He, D. Liu, L. Xu, D. Shi, E. Wang, and G. Zhang, A route toward digital manipulation of water nanodroplets on surfaces. *ACS Nano*, **8**(4), 3955-3960 (2014).

[7] D. A. Sanchez, Z. Dai, P. Wang, A. Cantu-Chavez, C. J. Brennan, R. Huang, and N. Lu, Mechanics of spontaneously formed nanoblisters trapped by transferred 2D crystals. *Proceedings of the National Academy of Sciences*, **115**(31), 7884-7889 (2018).

[8] F. Pizzocchero, L. Gammelgaard, B. S. Jessen, J. M. Caridad, L. Wang, J. Hone, P. Bøggild, and T. J. Booth, The hot pick-up technique for batch assembly of van der Waals heterostructures. *Nature Communications*, **7**, 11894 (2016).

[9] E. Khestanova, F. Guinea, L. Fumagalli, A. K. Geim, and I. V. Grigorieva, Universal shape and pressure inside bubbles appearing in van der Waals heterostructures. *Nature Communications*, **7**, 12587 (2016).

[10] R. D. Schulman, and K. Dalnoki-Veress, Droplets capped with an elastic film can be round, elliptical, or nearly square. *Physical Review Letters*, **121**(24), 248004 (2018).

[11] Y. Rao, S. Qiao, Z. Dai, and N. Lu, Elastic wetting: Substrate-supported droplets confined by soft elastic membranes. *Journal of the Mechanics and Physics of Solids*, **151**, 104399 (2021).

[12] M. E. R. Shanahan, and A. Carré, Spreading and dynamics of liquid drops involving nanometric deformations on soft substrates. *Colloids and Surfaces A: Physicochemical and Engineering Aspects*, **206**(1-3), 115-123 (2002).

[13] G. Pu, J. Guo, L. E. Gwin, and S. J. Severtson, Mechanical pinning of liquids through inelastic wetting ridge formation on thermally stripped acrylic polymers. *Langmuir*, **23**(24), 12142-12146 (2007).

[14] P. S. Yadav, P. Bahadur, R. Tadmor, K. Chaurasia, and A. Leh, Drop retention force as a function of drop size. *Langmuir*, **24**(7), 3181-3184 (2008).

[15] R. Tadmor, K. Chaurasia, P. S. Yadav, A. Leh, P. Bahadur, L. Dang, and W. R. Hoffer, Drop retention force as a function of resting time. *Langmuir*, **24**(17), 9370-9374 (2008).

[16] R. Tadmor, P. Bahadur, A. Leh, H. E. N'guessan, R. Jaini, and L. Dang, Measurement of lateral adhesion forces at the interface between a liquid drop and a substrate. *Physical Review Letters*, **103**(26), 266101 (2009).

[17] N. Gao, F. Geyer, D. W. Pilat, S. Wooh, D. Vollmer, H. J. Butt, and R. Berger, How drops start sliding over solid surfaces. *Nature Physics*, **14**(2), 191-196 (2018).

[18] Y. Jiang, Y. Sun, J. W. Drelich, and C. H. Choi, Topography-dependent effective contact line in droplet depinning. *Physical Review Letters*, **125**(18), 184502 (2020).

[19] R. Tadmor, Open Problems in Wetting Phenomena: Pinning Retention Forces. *Langmuir*, **37**, 6357-6372 (2021).

[20] D. G. Purdie, N. M. Pugno, T. Taniguchi, K. Watanabe, A. C. Ferrari, and A. Lombardo, Cleaning interfaces in layered materials heterostructures. *Nature Communications*, **9**, 5387 (2018).

[21] M. R. Rosenberger, H. J. Chuang, K. M. McCreary, A. T. Hanbicki, S. V. Sivaram, and B. T. Jonker, Nano-"squeegee" for the creation of clean 2D material interfaces. *ACS Applied Materials & Interfaces*, **10**(12), 10379-10387 (2018).

[22] Y. Hou, Z. Dai, S. Zhang, S. Feng, G. Wang, L. Liu, Z. Xu, Q. Li, and Z. Zhang, Elastocapillary cleaning of twisted bilayer graphene interfaces. *Nature Communications*, **12**, 5069 (2021).

[23] C. Ma, Y. Chen, and J. Chu, Time-dependent pinning of nanoblisters confined by two-dimensional sheets. Part 1: scaling law and hydrostatic pressure. *Langmuir*, submitted.

[24] K. S. Novoselov, A. K. Geim, S. V. Morozov, D. Jiang, Y. Zhang, S. V. Dubonos, I. V. Grigorieva, and A. A. Firsov, Electric field effect in atomically thin carbon films. *Science*, **306**(5696), 666-669 (2004).

[25] J. L. Hutter, and J. Bechhoefer, Calibration of atomic-force microscope tips. *Review of Scientific Instruments*, **64**(7), 1868-1873 (1993).

[26] O. L. Blakslee, D. G. Proctor, E. J. Seldin, G. B. Spence, and T. Weng, Elastic constants of compression-annealed pyrolytic graphite. *Journal of Applied Physics*, **41**(8), 3373-3382 (1970).

[27] K. Yue, W. Gao, R. Huang, and K. M. Liechti, Analytical methods for the mechanics of graphene bubbles. *Journal of Applied Physics*, **112**(8), 083512 (2012).

[28] P. Wang, W. Gao, Z. Cao, K. M. Liechti, and R. Huang, Numerical analysis of circular graphene bubbles. *Journal of Applied Mechanics*, **80**(4), 040905 (2013).

[29] G. R. Lester, Contact angles of liquids at deformable solid surfaces. *Journal of Colloid Science*, **16**(4), 315-326 (1961).

[30] M. E. R. Shanahan, The influence of solid micro-deformation on contact angle equilibrium. *Journal of Physics D: Applied Physics*, **20**(7), 945 (1987).

[31] A. Carré, J. C. Gastel, and M. E. Shanahan, Viscoelastic effects in the spreading of liquids. *Nature*, **379**(6564), 432-434 (1996).

[32] C. W. Extrand and Y. Kumagai, Contact angles and hysteresis on soft surfaces. *Journal of Colloid and Interface Science*, **184**(1), 191-200 (1996).

[33] R. Pericet-Cámara, A. Best, H. J. Butt, and E. Bonaccurso, Effect of capillary pressure and surface tension on the deformation of elastic surfaces by sessile liquid microdrops: an experimental investigation. *Langmuir*, **24**(19), 10565-10568 (2008).

[34] Y. S. Yu and Y. P. Zhao, Elastic deformation of soft membrane with finite thickness induced by a sessile liquid droplet. *Journal of Colloid and Interface Science*, **339**(2), 489-494 (2009).

[35] E. R. Jerison, Y. Xu, L. A. Wilen, and E. R. Dufresne, Deformation of an elastic substrate by a three-phase contact line. *Physical Review Letters*, **106**(18), 186103 (2011).

[36] A. Leh, H. E. N'guessan, J. Fan, P. Bahadur, R. Tadmor, and Y. Zhao, On the role of the three-phase contact line in surface deformation. *Langmuir*, **28**(13), 5795-5801 (2012).

[37] V. Charitatos and S. Kumar, A thin-film model for droplet spreading on soft solid substrates. *Soft Matter*, **16**(35), 8284-8298 (2020).

[38] M. E. R. Shanahan and P. G. De Gennes, Equilibrium of the triple line solid/liquid/fluid of a sessile drop. In *Adhesion 11* (eds. K. W. Allen), pp. 71-81. (Springer, Dordrecht, 1987).

[39] M. E. Shanahan and A. Carre, Anomalous spreading of liquid drops on an elastomeric surface. *Langmuir*, **10**(6), 1647-1649 (1994).

[40] A. Carré, and M. E. Shanahan, Direct evidence for viscosity-independent spreading on a soft solid. *Langmuir*, **11**(1), 24-26 (1995).

[41] M. E. R. Shanahan, The spreading dynamics of a liquid drop on a viscoelastic solid. *Journal of Physics D: Applied Physics*, **21**(6), 981 (1988).

[42] Z. Deng, A. Smolyanitsky, Q. Li, X. Q. Feng, and R. J. Cannara, Adhesion-dependent negative friction coefficient on chemically modified graphite at the nanoscale. *Nature Materials*, **11**(12), 1032-1037 (2012).

[43] H. E. N'guessan, A. Leh, P. Cox, P. Bahadur, R. Tadmor, P. Patra, R. Vajtai, P. M. Ajayan, and P. Wasnik, Water tribology on graphene. *Nature Communications*, **3**, 1242 (2012).

Abstract Graphics for Part 2